

ANGULAR MOMENTUM DISTRIBUTION OF HOT GAS AND IMPLICATIONS FOR DISK GALAXY FORMATION

D. N. CHEN AND Y. P. JING

Shanghai Astronomical Observatory, Partner Group of MPI für Astrophysik, Nandan Road 80, Shanghai 200030, China;
dnchen@center.shao.ac.cn, ypjing@center.shao.ac.cn

AND

KOJI YOSHIKAW

Research Center for the Early Universe (RESCEU), School of Science, University of Tokyo, Tokyo 113-0033, Japan;
kohji@utap.phys.s.u-tokyo.ac.jp

Received 2002 November 19; accepted 2003 July 11

ABSTRACT

We study the angular momentum profiles both for dark matter and for gas within virialized halos using a statistical sample of halos drawn from cosmological hydrodynamics simulations. Three simulations have been analyzed: one is the nonradiative simulation and the other two have radiative cooling. We find that the gas component, on average, has a larger spin and contains a smaller fraction of mass with negative angular momentum than its dark matter counterpart in the nonradiative model. As to the cooling models, the gas component shares approximately the same spin parameter as its dark matter counterpart, but the hot gas has a higher spin and is more aligned in angular momentum than dark matter, while the opposite holds for the cold gas. After the mass of negative angular momentum is excluded, the angular momentum profile of the hot gas component approximately follows the universal function originally proposed by Bullock et al. for dark matter, though the shape parameter μ is much larger for hot gas and is comfortably in the range required by observations of disk galaxies. Since disk formation is related to the distribution of hot gas that will cool, our study may explain the fact that the disk component of observed galaxies contains a smaller fraction of low angular momentum material than dark matter in halos.

Subject headings: cosmology: theory — dark matter — galaxies: formation — galaxies: halos — galaxies: spiral — galaxies: structure

1. INTRODUCTION

Angular momentum is one of the most important quantities that determine the structure of disk galaxies. In the popular hierarchical structure formation framework (White & Rees 1978), dark matter halos grow by means of gravitational instability and acquire angular momentum from tidal torques, and galaxies form through cooling of baryons within dark matter halos. In order to derive a density profile of the cooled gas, one needs three assumptions: (1) the specific angular momentum of gas is conserved during the collapse, (2) gas has the same initial angular momentum distribution as dark matter in a halo, and (3) either the disk density profile is assumed to be exponential as observed, or the angular momentum profile of dark matter halos is assumed. (Fall & Efstathiou 1980; Blumenthal et al. 1986; Dalcanton, Spergel, & Summers 1997; Jimenez et al. 1997; Mo, Mao, & White 1998; van den Bosch 1998; Avila-Reese & Firmani 2000).

The angular momentum of a halo is often parameterized by the dimensionless spin parameter

$$\lambda \equiv \frac{|\mathbf{J}||E|^{1/2}}{GM^{5/2}}, \quad (1)$$

where G is the gravitational constant, and \mathbf{J} , E , and M are the total angular momentum, energy, and mass of the halo, respectively (Peebles 1969). With the first two assumptions, it is clear that the disk scale length $R_d \propto \lambda R_{\text{vir}}$. The angular momentum of a halo is presumably acquired through tidal interactions with neighboring objects (Doroshkevich 1970; White & Rees 1984; Catelan & Theuns 1996; Lee & Pen

2000; Porciani, Dekel, & Hoffman 2002). In particular, with help of N -body simulations, the distribution of the halo spin parameter is found to be approximately lognormal with a median value of $\lambda \sim 0.05$ (Barnes & Efstathiou 1987). The implied distribution of disk scale length agrees reasonably well with observations (Mo, Mao, & White 1998; Cole et al. 2000; de Jong & Lacey 2000; van den Bosch et al. 2002; Shen et al. 2003).

Recently, Bullock et al. (2001, hereafter B2001) have determined the angular momentum distribution for individual dark matter halos in a concordance cold dark matter model. Their results imply that the dark halos have too much low angular momentum material to account for the observed typical exponential profiles of disk galaxies (B2001; van den Bosch 2001; van den Bosch, Burkert, & Swaters 2001), if the gas follows dark matter in the angular momentum distribution. It had been expected that warm dark matter assumption may resolve this problem, but recent studies (Chen & Jing 2002; Bullock, Kravtsov, & Colin 2002; Knebe et al. 2002) have not found any significant difference in the angular momentum profile between the two types of dark matter models. Chen & Jing (2002) and van den Bosch et al. (2002) also demonstrated that angular momentum of dark matter within a halo does not align well, and a significant fraction of dark matter is in counterrotation relative to the global spin of the halo. This implies that one should be cautious when the angular momentum of disk galaxies is compared with the angular momentum profile of Bullock et al. (2001) for dark matter halos. After the matter of negative angular momentum j is excluded (j is the angular momentum projected on the halo

spin axis), Chen & Jing (2002) showed that the angular momentum distribution is reasonably described by the universal profile suggested by B2001,

$$M(< j) = \frac{M(j > 0)\mu j}{j_0 + j}, \quad (2)$$

where $M(j > 0)$ is the total mass of positive angular momentum in the halo (the virial mass was in the original formula of B2001), $j_0 = (\mu - 1)j_{\max}$, and j_{\max} is the maximum specific angular momentum. The parameter μ indicates the shape of the profile, and a smaller μ means there is more mass of low angular momentum. Unless the material of low positive angular momentum is consumed in combination with that of negative angular momentum to form a bulge component as van den Bosch et al. (2002) suggested, it appears difficult to reconcile the exponential disk of spiral galaxies with CDM models.

Considering the above angular momentum problem, the first and second assumptions, which are essential ingredients of the standard paradigm for disk galaxy formation appear to be questionable. Van den Bosch et al. (2002) studied the angular momentum distribution of the gas in galactic dark halos at $z = 3$ in a nonradiative cosmological hydrodynamics simulation. They found that, on average, the gas and dark matter have the same distribution of the spin parameter and that their detailed angular momentum distributions in individual halos are very similar. Because the simulation box is only $10 h^{-1}$ comoving Mpc on each side, they cannot evolve the simulation to the redshift $z = 0$.

Because of its utmost importance, we analyze here the angular momentum distribution of halos in a set of three cosmological hydrodynamics simulations performed with a particle-particle-particle mesh smoothed particle hydrodynamics (P³MSPH) code (Yoshikawa et al. 2001). One simulation is nonradiative (or *adiabatic*), and the other two adopt different metallicities for gas and allow the gas to cool radiatively. From the two radiative cooling models, we can get information about the distribution of angular momentum in gas components with different temperatures. Since the disk formation is related to the distribution of hot gas before cooling, our division of gas into two components (hot and cold gas) becomes increasingly essential. The simulations were performed in a box of $75 h^{-1}$ Mpc, so most halos analyzed here are of mass of rich groups. Fortunately, it is generally believed that the angular momentum profile and spin parameter of halos depend on the halo mass very weakly (as dark matter simulations have shown; Lemson & Kauffmann 1999), so most results obtained here would also be applicable to galactic halos and disk formation. Our study here differs from that of van den Bosch et al. (2002) in several important aspects. First of all, in addition to one nonradiative simulation, we have two simulations with radiative cooling that enable us to do analysis for hot gas and cold gas separately. We do analysis for halos at redshift $z = 0$ and at group mass, and our simulations are generated with an independent code.

As will be seen, we find that the spin parameter of the hot gas component is nearly 20% larger than that of dark matter counterpart in all the three models, including the nonradiative model. The hot gas component has much less mass with negative angular momentum j than dark matter component, that is, the angular momentum of the hot gas is significantly more aligned than that of dark matter. Since disk formation

is related to the distribution of hot gas that will cool, these results will have interesting implications for galactic disk formation.

We present our methods for computing the angular momentum in § 2. In § 3, the results of our analysis are presented. We give our conclusions and discussion in § 4.

2. METHOD

2.1. Numerical Simulations

The cosmological simulations were generated with a P³M SPH code. A description of the code is presented in Yoshikawa, Jing, & Suto (2000). All the present runs employ $N_{\text{DM}} = 128^3$ dark matter particles and the same number of gas particles. The model is derived from a spatially flat low-density cold dark matter universe with the cosmological density parameter $\Omega_0 = 0.3$, the cosmological constant $\lambda_0 = 0.7$, and the Hubble constant, in units of $100 \text{ km s}^{-1} \text{ Mpc}^{-1}$, $h = 0.7$. The power-law index of the primordial density fluctuation is set to $n = 1$. The baryon density parameter is $\Omega_b = 0.015 h^{-2}$ and the amplitude σ_8 (the rms top hat density fluctuation of radius $8 h^{-1}$ Mpc at the present time) of the linear density power spectrum is 1.0. The simulation box is $75 h^{-1}$ Mpc wide, the initial condition is created at redshift $z = 36$, and the simulations are evolved to $z = 0$. The gas component is treated as an ideal gas with an adiabatic index $\gamma = 5/3$ and is either nonradiative or allowed to cool radiatively. The nonradiative simulation is also called adiabatic simulation according to conventions in the literature. For the two cooling runs, the cooling rate of Sutherland & Dopita (1993) is adopted with the metallicity $[\text{Fe}/\text{H}] = -0.5$ and -1.5 , respectively. The cooling run with $[\text{Fe}/\text{H}] = -0.5$ is used by Yoshikawa et al. (2001) to study the clustering properties of galaxies.

In Figure 1, we give the histogram for the percentage of cold gas (i.e., gas with temperature below 10^6 K) within halos as a function of the halo gas mass. Here we use the number of gas particles N_{gas} to denote the gas mass. The upper panel is for the $[\text{Fe}/\text{H}] = -1.5$ model, while the lower panel is for the $[\text{Fe}/\text{H}] = -0.5$ model. The higher metallicity means a higher cooling rate; thus, more cold gas particles, as the figure shows. For halos of 3000 particles, there are nearly 60% of their gas particles cooled in the $[\text{Fe}/\text{H}] = -1.5$ model, and this percentage becomes 70% in the metal-richer $[\text{Fe}/\text{H}] = -0.5$ model. For halos of 10^4 particles, there are approximately 55% and 45% of gas particles cooled in the $[\text{Fe}/\text{H}] = -0.5$ and -1.5 models, respectively. For the most massive halos (about 2×10^4 particles), these percentages become 39% and 23%, respectively. Because the hot gas percentages are different in the two cooling models, we will test if our conclusions with regard to the angular momentum distribution are sensitive to the cooling rate (or the fraction of hot gas).

2.2. Identification of Dark Halos

The halos are identified from the simulations using the potential minimum method as described in Jing & Suto (2002). The method uses the spherical overdensity criterion to define a halo; thus, the halos have an overdensity $\Delta_c(z)$ according to Kitayama & Suto (1996) and Bryan & Norman (1998). For the cosmological model in this paper, $\Delta_c(z) = 101$ at $z = 0$.

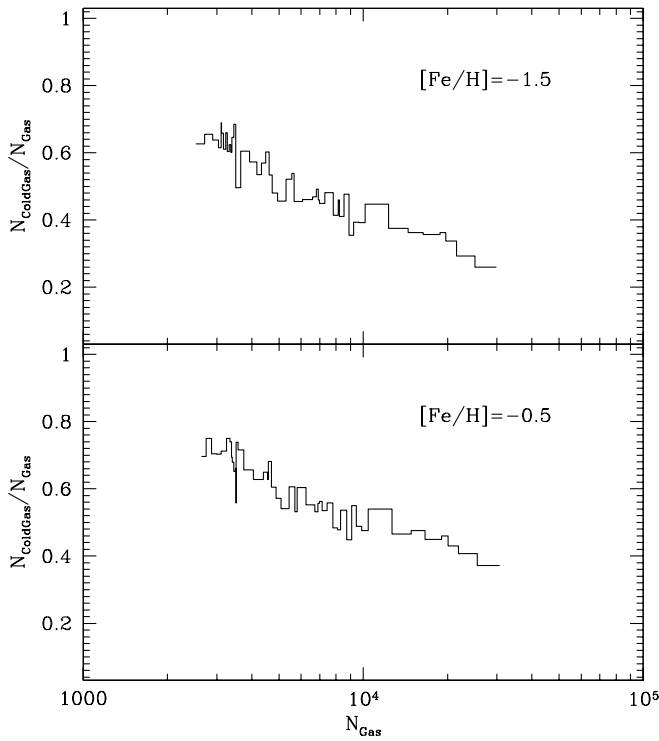


Fig. 1.—Percentage of cold gas as a function of halo gas mass in units of the gas particle mass. *Upper panel:* $[\text{Fe}/\text{H}] = -1.5$ model. *Lower panel:* $[\text{Fe}/\text{H}] = -0.5$ model.

In order to study the angular momentum distribution accurately, we select halos that at least have 3000 gas particles and 3000 dark matter particles. There are 48, 47, and 46 halos in the nonradiative model, $[\text{Fe}/\text{H}] = -0.5$ model and $[\text{Fe}/\text{H}] = -1.5$ model, respectively. The halos are ordered according to their dark matter mass. Since the initial density perturbation is the same in the three simulations, we can find the correspondence among the halos in different simulations. The ordering number of the same halo may vary slightly in the three models, because the cooling process can affect the distribution of dark matter. We compare the angular momentum distribution for the corresponding halos in different cooling models.

2.3. Angular Momentum

The aim of the paper is to study the angular momentum distribution of gas and dark matter in halos. We first determine the global angular momentum \mathbf{J} for each matter component (e.g., dark matter, gas, or hot gas) in a halo and define the z -axis for this matter component as pointing to the direction of \mathbf{J} . The global angular momenta are measured as follows:

$$\mathbf{J}_{\text{gas,DM}} = \sum_{i=1}^{N_{\text{gas,DM}}} m_i \mathbf{r}_i \times \mathbf{v}_i, \quad (3)$$

where \mathbf{r}_i and \mathbf{v}_i are the position and velocity of the i th gas or dark matter particle with respect to the halo center of mass. Following Mo, Mao, & White (1998; see also B2001), we measure the spin parameter λ for the gas and dark matter

components using

$$\lambda_{\text{gas,DM}} = \frac{J_{\text{gas,DM}}}{\sqrt{2} M_{\text{gas,DM}} V_c r_v}, \quad (4)$$

where V_c is the circular velocity at the virial radius r_v .

To quantify the misalignment between the angular momenta of the gas and dark matter components, we compute the angle

$$\theta = \arccos \left(\frac{\mathbf{J}_{\text{gas}} \times \mathbf{J}_{\text{DM}}}{|\mathbf{J}_{\text{gas}}| |\mathbf{J}_{\text{DM}}|} \right) \quad (5)$$

between their angular momentum vectors. The same formula has been adopted by van den Bosch et al. (2002), so our measurement results for the θ distribution in the nonradiative model can be compared with theirs.

The angular momentum distribution measures the fraction of the mass in a halo that has specific angular momentum greater than j . Although it seems straightforward to determine this quantity from velocity and position of particles, the interpretation of such a measured result is far less straightforward in the framework of disk galaxy formation. The main reason is that dark matter is collisionless, so dark matter particles move rapidly and randomly in addition to a slow global rotation. The random motion of gas particles should be much reduced by the shocks but may not be completely suppressed if the shocks still exist.

The cell method for measuring the angular momentum distribution, proposed by B2001, intends to eliminate the effect of random motion of the particles (see also Chen & Jing 2002). They divide each halo in the spherical coordinates (r, θ, ϕ) . Each halo is first divided into 10 shells such that there are approximately the same number of particles in each shell. Then each shell is divided into six azimuthal cells of equal volume. The two cells with the same r and $\sin \theta$ above and below the equatorial plane are merged; therefore, there are 30 cells in each halo. We will adopt this cell division method for our analysis and call it as $10 \times 3 \times 1$ cell method. The cells thus defined are not contiguous. In view of this possible problem and in order to see whether a special cell division of a halo can have impacts on our result, we adopt two additional cell divisions. One is the so-called $10 \times 6 \times 1$ method. The difference of this division from the $10 \times 3 \times 1$ cell method is that the two cells above and below the equatorial plane are not merged, so the cells are contiguous. The other is the $5 \times 6 \times 1$ cell method, which is the same as the $10 \times 6 \times 1$ method, except that the halo is divided into only five shells in radius.

We estimate the error of the special angular momentum j in the same way as in Chen & Jing (2002),

$$\sigma_j = \frac{rv_c(r)}{\sqrt{N_c}}, \quad (6)$$

where N_c is the particle number in the cell, and r is the mean distance of the cell from the halo center. The error estimated above is likely an upper limit on the scatter because the motion of particles is not completely random.

As we mentioned earlier, van den Bosch et al. (2002) have analyzed the angular momentum distribution for a nonradiative SPH/ N -body simulation. Considering that the gas particles are collisional, they computed the angular momentum distribution for gas based on the velocity of individual gas particles. To distinguish their method with the cell

method, we will call their method as the particle method. For a uniformly rotating sphere of gas, one would expect that both methods yield the same angular momentum distribution. But for a halo that is in continuous merger in the hierarchical clustering, the two methods may produce different results. For example, in the particle method, the shocks generated during an merger may lead to a certain degree of local misalignment of the angular momentum. Such local misalignment may not be wanted to show up in the present analysis, as it will probably be shocked away later. The cell method can avoid this complication to a large extent, but the results may depend on the way of dividing halos. It is therefore difficult to assess which method is superior. We adopt both methods in order to make proper comparisons with those of B2001 and van den Bosch et al. (2002). Since we do not add a random motion to the motion of gas particles, our results for the angular momentum distribution should be compared with those without superscript v in van den Bosch et al. (2002).

3. RESULTS

3.1. The Global Angular Momentum

Figure 2 and 3 shows the distribution of the angle θ between the global angular momentum vectors of dark mat-

ter and gas components. The first column is for our cooling model with metallicity $[\text{Fe}/\text{H}] = -0.5$. Among the three panels in the column, the lower one is for cold gas, the middle one for hot gas, and the upper one for hot and cold gas together. The mean value of θ is $40^\circ.5$, $21^\circ.0$, and $25^\circ.0$ for the three components, respectively. The middle column has the same layout as the left one but for the $[\text{Fe}/\text{H}] = -1.5$ model, with the mean $22^\circ.8$, $20^\circ.9$, and $38^\circ.9$ from top to bottom. Since there is no cooling in the nonradiative model, the right column only plots for hot gas, and the mean θ is $23^\circ.5$. Our results can be compared with Figure 3 of van den Bosch et al. (2002). Their mean value of θ for the nonradiative model is about 36° , a bit larger than ours. This is expected, because they included all halos with more than 100 dark matter particles in their analysis; thus, the discreteness effect of particles is more pronounced in their sample. They showed that the angle θ increases with decreasing halo mass M_{vir} , and the θ at the low end of halo mass may have been affected by the discreteness effect. We do not find any relation between θ and M_{vir} in our sample (Fig. 4) because we include only very massive halos. However, the mean misalignment angle is found to decrease with increasing spin parameter (see Fig. 3), in agreement with van den Bosch et al. (2002). This relation may partly be attributed to the particle discreteness again, for the discreteness has relatively

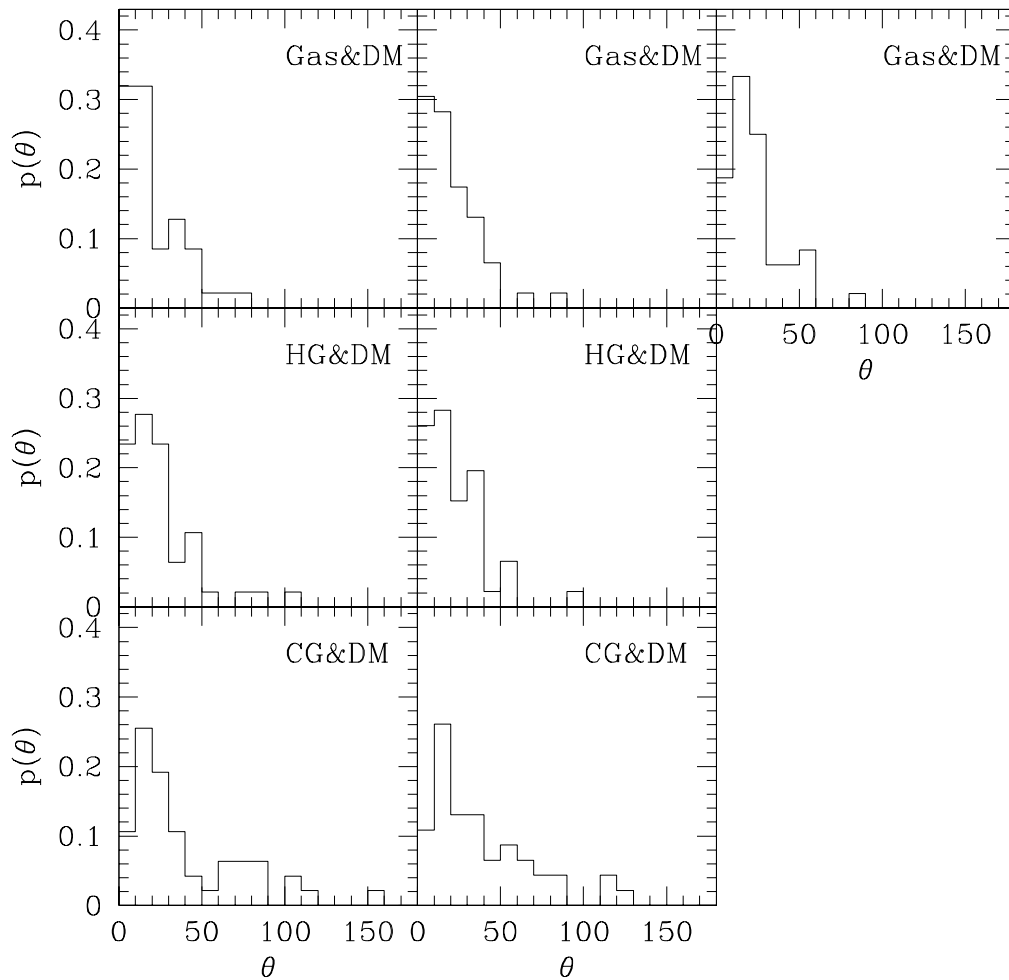


FIG. 2.—Distribution of angle θ between the total angular momentum vectors of dark matter and the gas. *Left column:* $[\text{Fe}/\text{H}] = -0.5$ model. *Middle column:* $[\text{Fe}/\text{H}] = -1.5$ model. *Right column:* Nonradiative model.

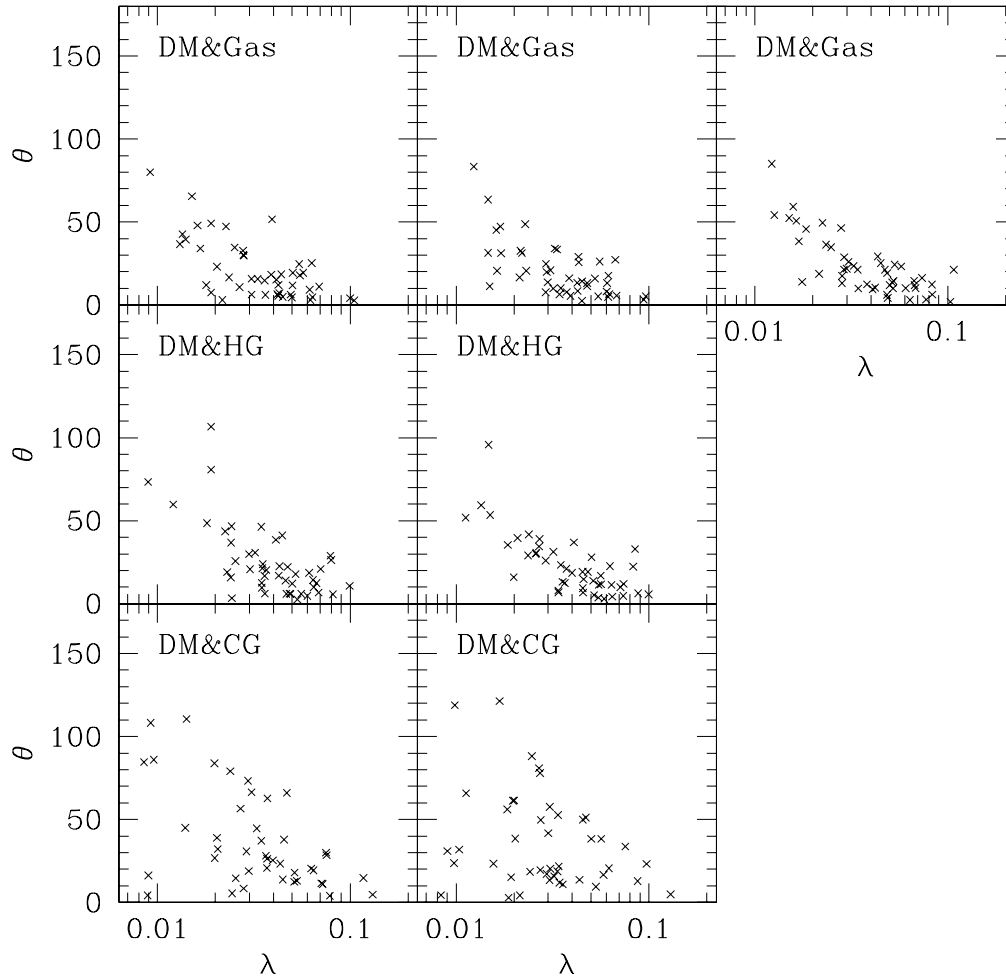


FIG. 3.—Misalignment θ of the angular momentum vectors between dark matter and a gas component as a function of the spin parameter λ of dark matter. The gas component is indicated in each panel. *Left column*: $[\text{Fe}/\text{H}] = -0.5$ model. *Middle column*: $[\text{Fe}/\text{H}] = -1.5$ model. *Right column*: Nonradiative model.

less effect on high spin halos. Overall, our results for the nonradiative model are in good agreement with those of van den Bosch et al. (2002), in spite of the difference in many aspects between the simulations used in the two studies. The misalignment angle is affected very slightly by the cooling process, although the hot component aligns slightly better with dark matter in angular momentum than the cold component. A straightforward conclusion is that the angular momentum vector of gas or hot gas lies in an angle of 20° with that of dark matter, and this misalignment should be considered in interpreting observations, e.g., the alignment correlation of disk galaxies (Lee & Pen 2001).

Figure 5 plots the histogram of the spin parameter λ separately for each matter component. The distributions are well fitted by the lognormal function,

$$p(\lambda)d\lambda = \frac{1}{\sqrt{2\pi}\sigma_\lambda} \exp\left[-\frac{\ln^2(\lambda/\lambda_0)}{2\sigma_\lambda^2}\right] \frac{d\lambda}{\lambda}. \quad (7)$$

The σ_λ and λ_0 for each component are given in the figure. The top panels are for the nonradiative model, which can be compared with Figure 1 of van den Bosch et al. (2002). We get a bit smaller λ_0 for our dark matter component than its nonradiative gas counterpart (i.e., 0.032 vs. 0.038). The middle row of panels is for the $[\text{Fe}/\text{H}] = -0.5$ model, but with a

more detailed classification for the gas components. We note that the total gas component shares approximately the same λ_0 and σ_λ as dark matter for this cooling model, while hot gas presents a larger λ_0 than both total gas and dark matter components. Just as one would expect, cold gas has the smallest λ_0 . Qualitatively, the same results have been found for the $[\text{Fe}/\text{H}] = -1.5$ model, as shown in the bottom panels.

Figure 6 presents a one-to-one comparison of the spin parameter λ between gas and dark matter. The left column is for total gas and dark matter and from top to bottom panels are the nonradiative, $[\text{Fe}/\text{H}] = -1.5$, and $[\text{Fe}/\text{H}] = -0.5$ models, respectively. We could arrive at conclusion that, on average, the gas component hosts a larger spin parameter than its dark matter counterpart for the nonradiative model (Fig. 5, upper panel). But this tendency becomes weaker when the cooling enhances. For the model with the highest cooling rate (i.e., the $[\text{Fe}/\text{H}] = -0.5$ model; bottom panel), the gas and dark matter share nearly the same spin. From the right column, however, we see that the hot gas generally processes a higher spin than dark matter, while the cold gas has a lower spin. On average, the spin parameter of the hot gas component is 20% to 30% higher than that of dark matter. The difference between these two components is significant at a confidence level of $80\% \pm 10\%$ in the three models,

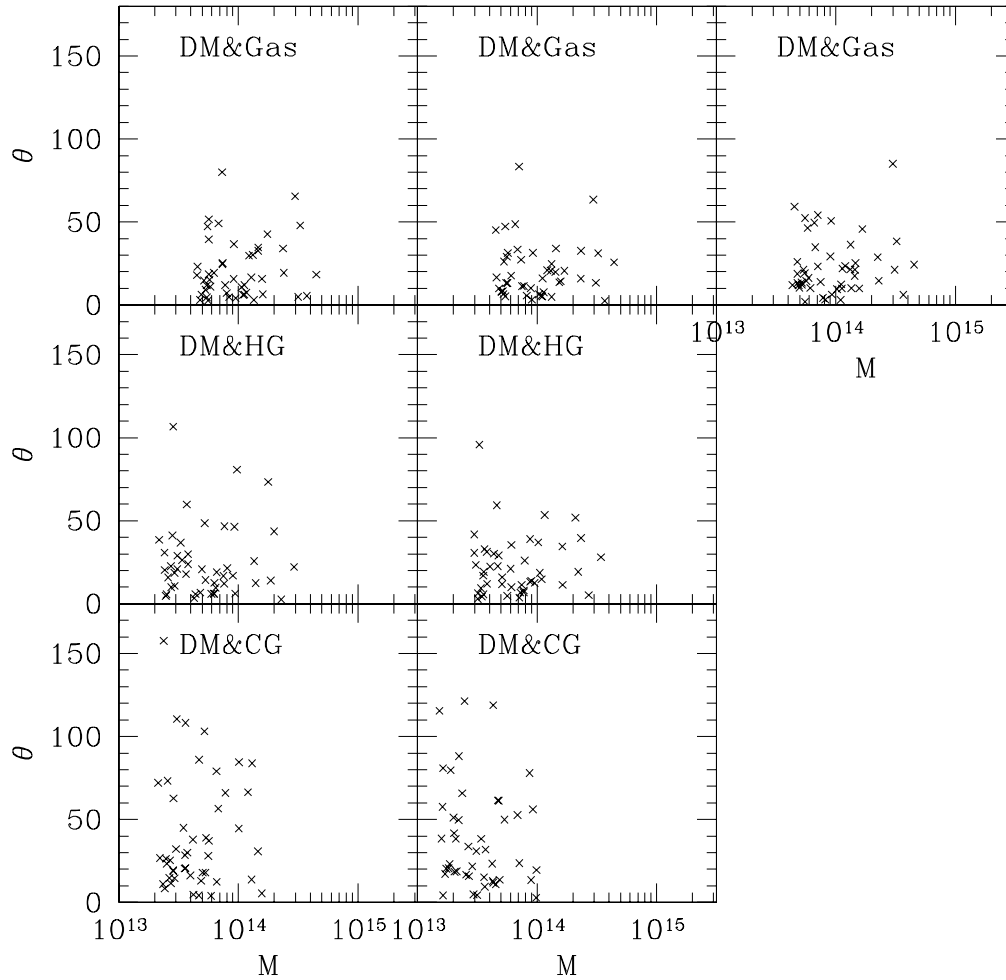


FIG. 4.—Same as Fig. 3, except that the misalignment angle is plotted as a function of halo mass M (the sum of dark matter mass and gas mass)

as the Kolmogorov-Smirnov tests show (see Table 1). The λ distributions of dark matter and gas in the cooling models are consistent with being drawn from the same parent distribution (see also Fig. 5 and Table 1).

3.2. Angular Momentum Distribution

Now we measure the angular momentum distribution based on the cell division method. Figure 7 shows the results for six halos randomly selected from the nonradiative model. The left two columns present the angular momentum distribution for dark matter (Fig. 7, *left*) and gas (Fig. 7, *right*) using $5 \times 6 \times 1$ cell method. While the middle two

and the right two columns are for $10 \times 6 \times 1$ and $10 \times 3 \times 1$ cell divisions, respectively. The basic properties of these six halos are listed in Table 3. Columns (7) and (8) of Table 4 list the shape parameter μ for each halo, which is obtained by fitting the data with equation (2). For a small fraction of halos (e.g., halo 06 in Table 4), the fitted parameter μ shows a significant variation among different cell divisions, while for most halos, the measured shape parameter μ changes only slightly when the different cell divisions are applied (e.g., col. [7] in Table 4). Especially, relative values of the parameter μ among the halos nearly do not change with cell divisions, indicating that the results are quite robust to the cell divisions.

We have measured the shape parameter μ for all halos in the three simulations, using the three division methods. For the gas, we also consider the hot and cold components separately. Since there is a considerable amount of misalignment in the angular momentum of cold gas (see below) and its angular momentum profile often can not be described by equation (2), we do not measure the μ parameter for the cold gas. Our measured results for the hot gas and dark matter are presented in Figure 8. Generally speaking, either gas in the nonradiative model or hot gas in the cooling models has a much larger μ value than their dark matter counterpart, indicating that there is relatively less mass of low angular momentum in hot gas than in dark matter. The median

TABLE 1
THE PROBABILITY OF TWO λ DISTRIBUTIONS DRAWN FROM THE SAME PARENT DISTRIBUTION

Model	Components	Probability
Nonradiative.....	DM vs. GAS	0.2199
[Fe/H] = -0.5.....	DM vs. GAS	0.8117
	DM vs. HG	0.3206
	DM vs. CG	0.4662
[Fe/H] = -1.5.....	DM vs. GAS	0.6246
	DM vs. HG	0.1229
	DM vs. CG	0.6245

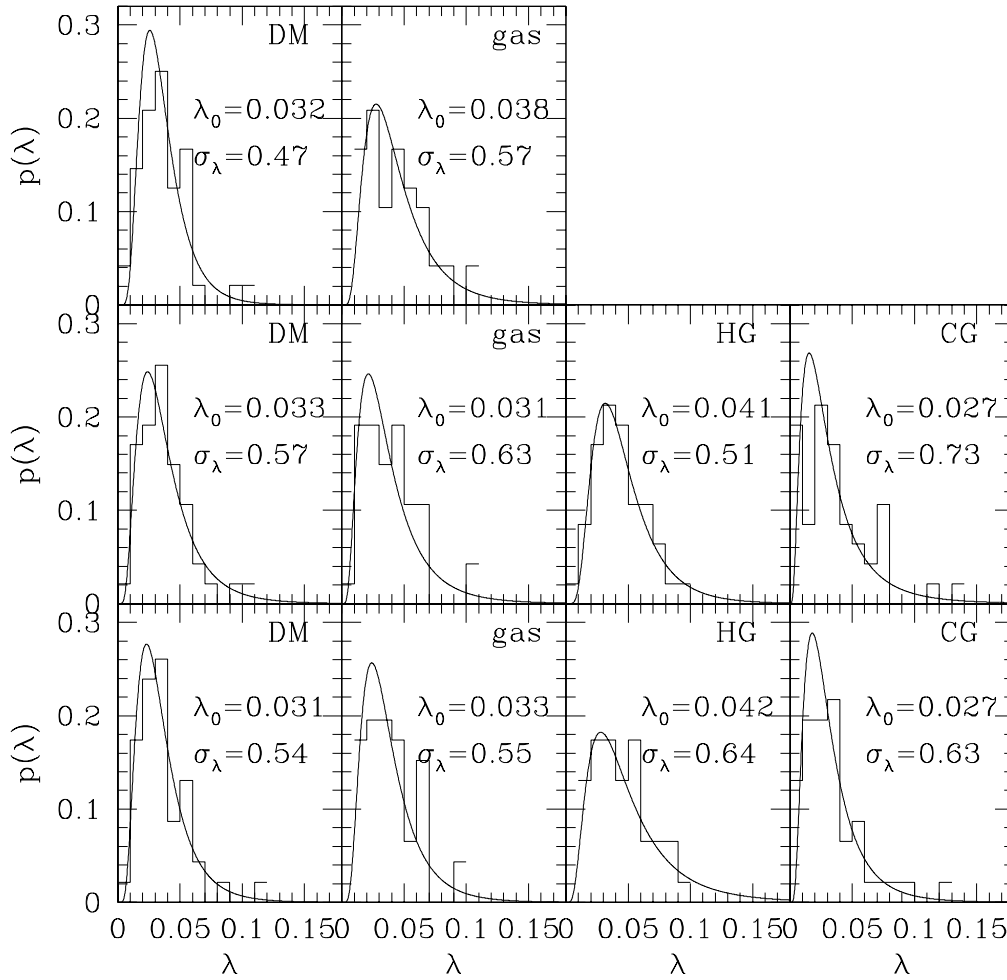


FIG. 5.—The λ distributions of dark matter and gas components. *Solid curves*: Best-fit lognormal distributions of eq. (7). HG: Hot gas. CG: Cold gas. *Upper panels*: Nonradiative model. *Middle panels*: $[\text{Fe}/\text{H}] = -0.5$ model. *Lower panels*: $[\text{Fe}/\text{H}] = -1.5$ model.

value of μ is around 2 for hot gas in the two cooling models, compared to 1.3 for dark matter. The difference of the angular momentum profiles between the two components is significant according to the Kolmogorov-Smirnov test (Table 2). This conclusion does little depend on the cell divisions. We will discuss its implications for disk galaxy formation in next section.

In order to quantify how much mass in halos is contained in negative j cells and to see whether there exists any relation

between the negative j mass fraction and the spin parameter λ , we measure the fraction of negative j mass, f , as a function of the spin parameter λ . The results based on the $5 \times 6 \times 1$ cell method are presented in the lower panel of Figure 9. It is interesting to note that while dark matter and gas in halos have a similar fraction of mass contained in negative j cells, the hot gas component contains much less negative j mass. The median value of f for the hot gas in the two cooling models is smaller than 0.1, i.e., there is very little hot gas that is in counterrotation in the cooling models. For the nonradiative model, we also see a much smaller fraction of

TABLE 2
THE PROBABILITY OF TWO μ DISTRIBUTIONS DRAWN FROM THE SAME PARENT DISTRIBUTION

Model	Components	Cell	Probability
Nonradiative.....	DM vs. GAS	$5 \times 6 \times 1$	9.9×10^{-3}
		$10 \times 6 \times 1$	6.2×10^{-2}
		$10 \times 3 \times 1$	6.7×10^{-2}
$[\text{Fe}/\text{H}] = -0.5$	DM vs. HG	$5 \times 6 \times 1$	5.9×10^{-5}
		$10 \times 6 \times 1$	7.3×10^{-8}
		$10 \times 3 \times 1$	5.9×10^{-5}
$[\text{Fe}/\text{H}] = -1.5$	DM vs. HG	$5 \times 6 \times 1$	1.3×10^{-2}
		$10 \times 6 \times 1$	8.0×10^{-4}
		$10 \times 3 \times 1$	2.6×10^{-5}

TABLE 3
GLOBAL PARAMETERS OF HALOS IN FIGURE 7

Identification (1)	N_{DM} (2)	N_{gas} (3)	λ_{DM} (4)	λ_{gas} (5)	$\cos \theta$ (6)
06.....	15679	13919	0.019	0.029	0.876
13.....	9031	8368	0.066	0.061	0.984
22.....	7509	6890	0.035	0.038	0.976
28.....	5502	5064	0.047	0.077	0.998
33.....	3844	3435	0.023	0.015	0.610
41.....	3844	3678	0.056	0.074	0.960

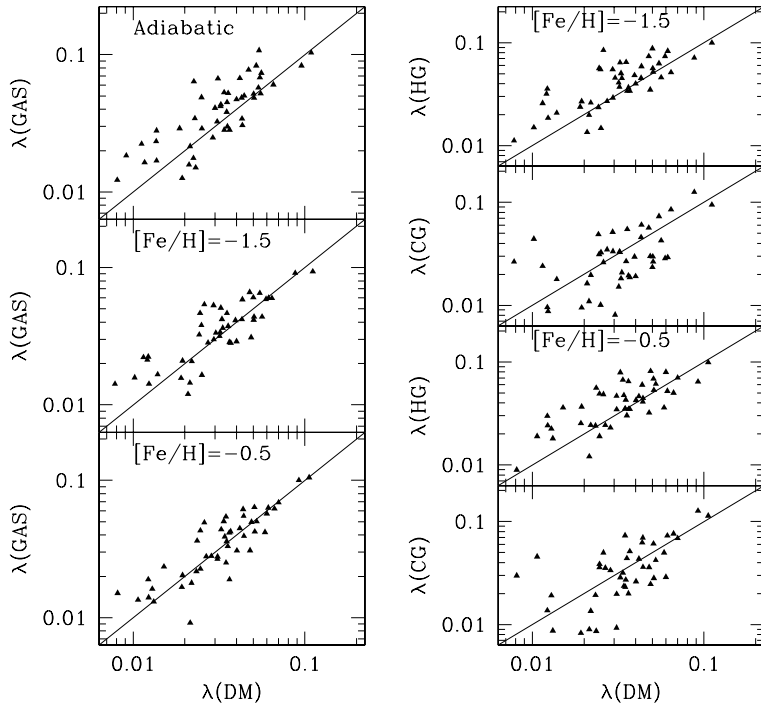


FIG. 6.—Spin parameter λ of different gas components vs. that of dark matter component in the three models

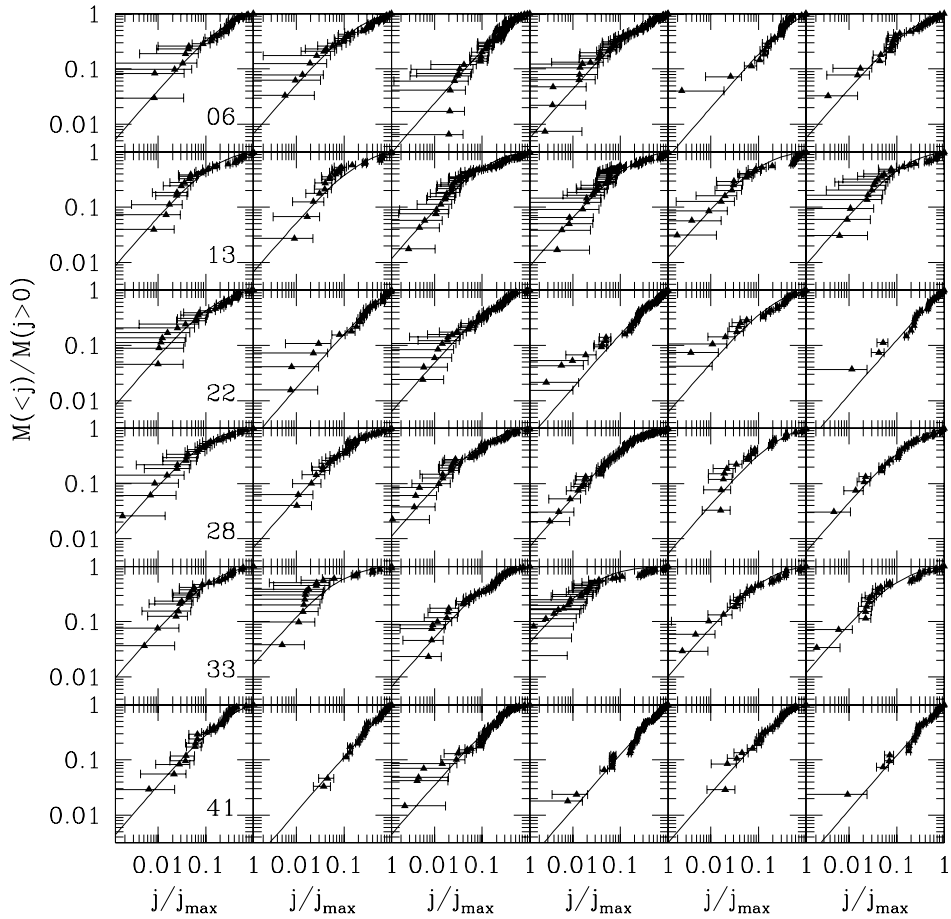


FIG. 7.—Mass distribution of specific angular momentum of six randomly selected halos in the nonradiative model. *Left to right*: First two columns are for dark matter. *Left*: Gas component. *Right*: $5 \times 6 \times 1$ cell method. *Middle and right columns*: $10 \times 6 \times 1$ cell method and the $10 \times 3 \times 1$ cell method, respectively.

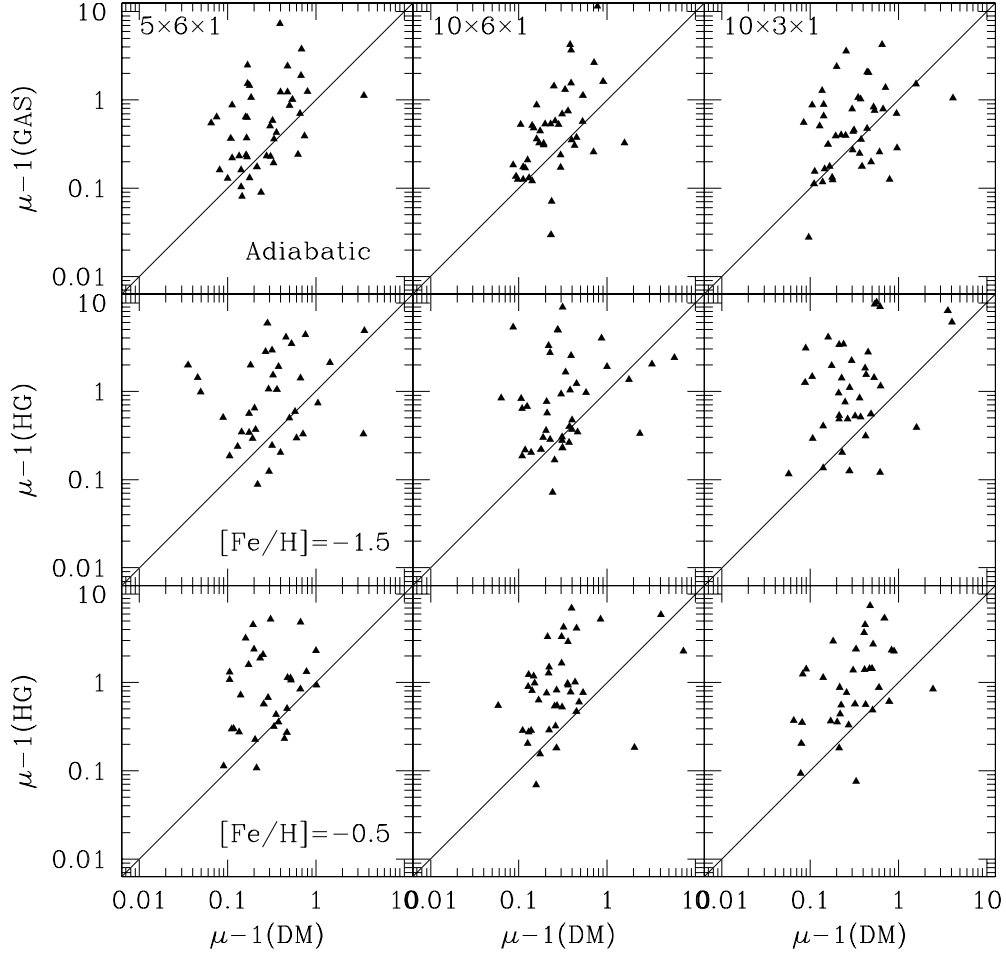


FIG. 8.—Shape parameter μ of different gas components vs. that of dark matter component. *Top*: Nonradiative model using different cell method. *Middle*: $[\text{Fe}/\text{H}] = -0.5$ model. *Bottom*: $[\text{Fe}/\text{H}] = -1.5$ model.

TABLE 4
COMPARISON OF THE FRACTION OF NEGATIVE j MASS AND THE SHAPE PARAMETER μ OF HALOS IN FIGURE 7

Identification (1)	f_{DM}^{a} (2)	$f_{\text{gas}}^{\text{a}}$ (3)	Cell (4)	f_{DM}^{b} (5)	$f_{\text{gas}}^{\text{b}}$ (6)	μ_{DM} (7)	μ_{gas} (8)
			$5 \times 6 \times 1$	0.077	0.0	1.31	1.23
06.....	0.44	0.32	$10 \times 6 \times 1$	0.18	0.024	1.70	1.28
			$10 \times 3 \times 1$	0.12	0.024	1.97	1.29
			$5 \times 6 \times 1$	0.17	0.25	1.17	1.23
13.....	0.40	0.32	$10 \times 6 \times 1$	0.15	0.24	1.12	1.17
			$10 \times 3 \times 1$	0.13	0.13	1.11	1.16
			$5 \times 6 \times 1$	0.070	0.10	1.18	2.45
22.....	0.41	0.28	$10 \times 6 \times 1$	0.16	0.11	1.25	2.43
			$10 \times 3 \times 1$	0.10	0.14	1.26	4.57
			$5 \times 6 \times 1$	0.19	0.0	1.11	1.22
28.....	0.43	0.14	$10 \times 6 \times 1$	0.24	0.0	1.12	1.21
			$10 \times 3 \times 1$	0.19	0.0	1.30	1.27
			$5 \times 6 \times 1$	0.18	0.39	1.15	1.08
33.....	0.44	0.44	$10 \times 6 \times 1$	0.28	0.42	1.23	1.03
			$10 \times 3 \times 1$	0.17	0.19	1.14	1.12
			$5 \times 6 \times 1$	0.033	0.0	1.39	4.29
41.....	0.38	0.12	$10 \times 6 \times 1$	0.076	0.0	1.39	4.68
			$10 \times 3 \times 1$	0.055	0.0	1.66	5.26

^a Using the particle method.

^b Using the cell method.

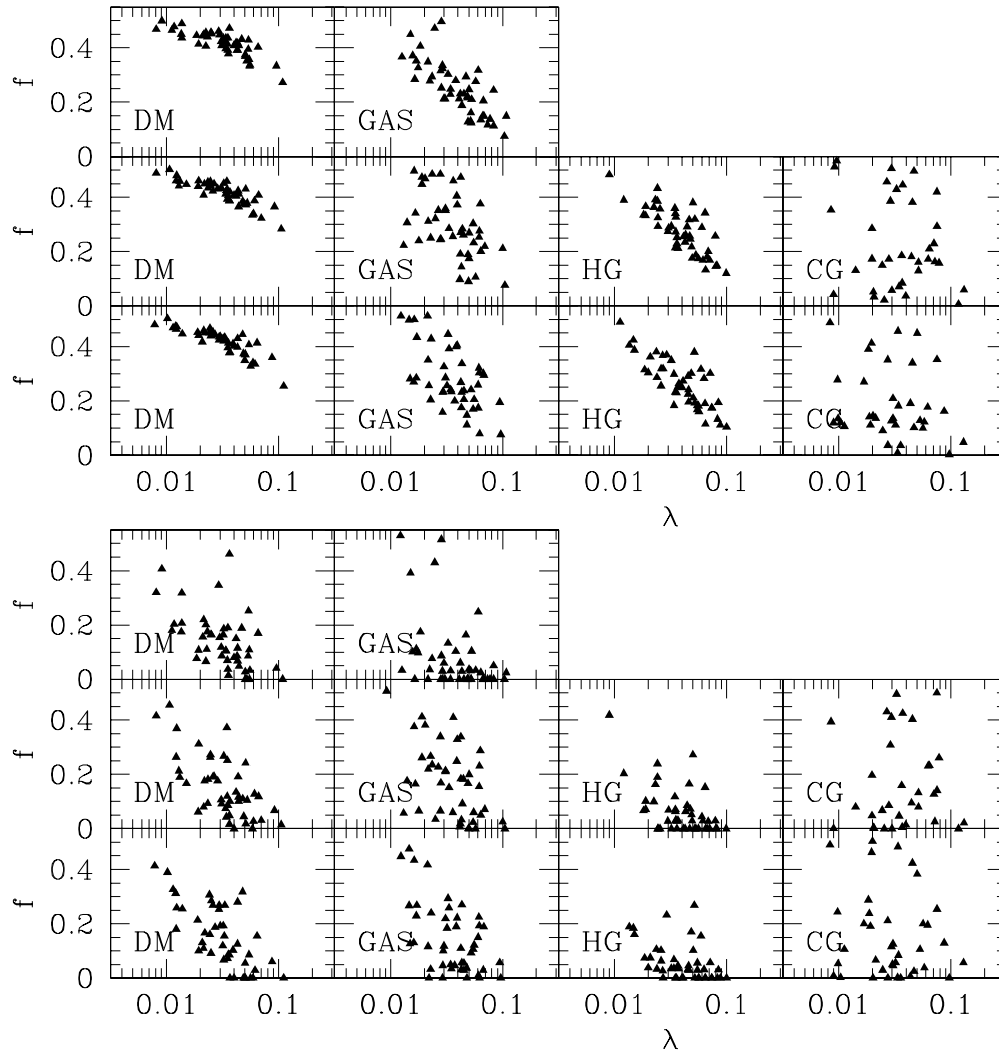


FIG. 9.—Fraction of negative j mass in dark matter or in gas components as a function of the spin parameter λ of dark matter. *Both panels, top to bottom:* Nonradiative, $[\text{Fe}/\text{H}] = -0.5$, and $[\text{Fe}/\text{H}] = -1.5$ models, respectively. *Upper panels:* Particle method. *Lower panels:* $5 \times 6 \times 1$ cell method.

negative j mass in the hot gas than in dark matter, though the fraction is slightly higher than that in the cooling models. These results again are robust to the cell divisions, as shown by Figure 10.

4. CONCLUSIONS AND DISCUSSION

We have presented a detailed study of the specific angular momentum (j) profile for dark matter and for gas components within dark halos, using a set of cosmological N -body hydrodynamics simulations. We have used the cell division method to measure the angular momentum profile. Three simulations have been analyzed, one is the nonradiative simulation, and the other two have radiative cooling. We find that the gas component, on average, has a larger spin and contains less mass with negative angular momentum than its dark matter counterpart in the nonradiative model. As to the cooling models, the gas component shares approximately the same spin value as its dark matter counterpart, but the hot gas has a higher spin parameter and is more aligned in angular momentum than the dark matter, while the opposite holds for the cold gas. After the mass of nega-

tive angular momentum is excluded, the angular momentum profile of the hot gas component approximately follows the universal function proposed by Bullock et al., though the shape parameter μ is around 2 for hot gas, compared to the typical value 1.25 for dark matter. Our results are quite robust to the variation of cell divisions. It is interesting to note that $\mu \approx 2$ is needed to explain the observed disk exponential profiles of late-type galaxies (Bullock et al. 2001; van den Bosch 2001).

Our result has interesting implications for the formation of galactic disks. In the framework of hierarchical clustering, halos are formed through mergers of smaller halos and accretion of surrounding material. As Wechsler et al. (2002) and Zhao et al. (2003) recently showed, the growth of a galactic halo can be generally divided into two phases, major merger phase ($z > 2.5$) and slow accretion phase ($z < 2.5$). In the major merger phase, the halo merges are very frequent and violent; thus, galactic disks are not expected to form in this phase. In the slow accretion phase, halos grow much more quietly, and disks are expected to form in this phase if there is hot gas within the halos that can cool down gradually. Cold gas might exist in the

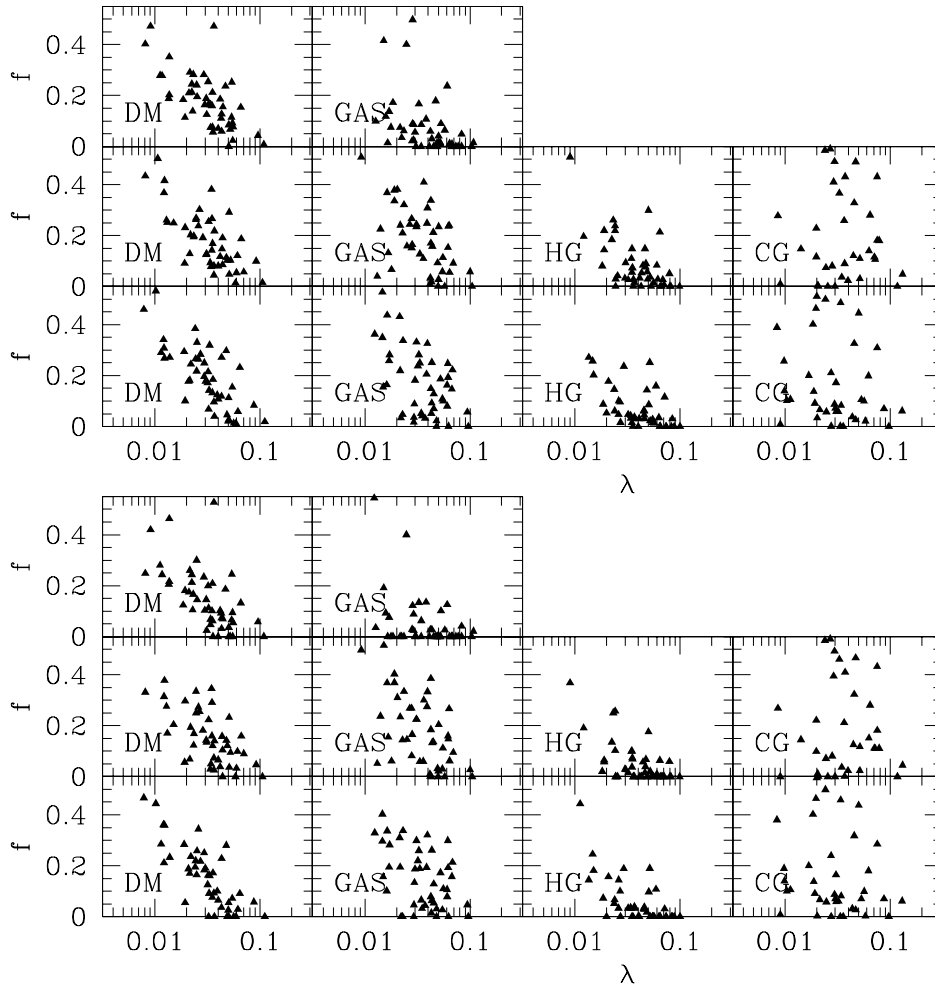


FIG. 10.—Same as Fig. 9, but using the $10 \times 6 \times 1$ (upper panel) and $10 \times 3 \times 1$ (lower panel) cell methods, respectively

halos before the slow accretion phase, but this cold gas likely forms the bulge component during the major merge phase; therefore, the galactic disk formation is related to the distribution of hot gas that will cool during the slow accretion phase. The halos studied in this work are typically in the slow accretion phase according to Zhao et al. (2003); thus, the hot gas may correspond to that forming galactic disks.

If the hot gas in halos of galactic mass follows the angular momentum profile of the hot gas of group halos in our cooling models, the formed disk would look like what observed in disk galaxies. This is demonstrated by Figure 11, which presents the fraction $p(l)dl$ of the hot gas (in all gas) that has angular momentum in $l \sim l + dl$, where $l = j/j_{\text{tot}}$ and j_{tot} is the mean specific angular momentum of the hot gas. The halos are selected from the simulations randomly from the three models. This figure can be compared with the observation of disk galaxies in van den Bosch (2002, his Fig. 1). The distributions of hot gas in the two cooling models look much like those of disk galaxies of van den Bosch et al. (2002). The dotted lines denote the Bullock profile of $\mu = 1.25$, a typical profile for dark matter. This profile was found to contain too much low angular momentum mass compared with the observations of disk galaxies (Bullock et al. 2001; van den Bosch 2001) and does not describe well the hot gas in our cooling simulations either. The solid lines

represent the Bullock profile of $\mu = 1.8$ multiplied by the typical hot gas fractions (of all gas) 1, 0.65, and 0.55, respectively, from the top to bottom panels, respectively, and the hot gas in our cooling models is approximately described by these profiles. We note that the observations of disk galaxies do require a typical $\mu = 1.8$ (Bullock et al. 2001; van den Bosch 2001). Our results indicate that the global rotation of hot gas is slightly faster than that of dark matter. This may also have an interesting consequence on the Sunyaev-Zel'dovich effect measurement of massive clusters (Cooray & Chen 2002).

We realize that the mechanism for keeping hot gas in our cooling simulations must be different from that is operating in galactic halos in the universe. In our simulations, because the halos are more massive than galaxy groups, around 50% of gas naturally remains in the hot gas phase. However, for galactic halos, because they were formed earlier and thus have higher density, only certain feedback mechanisms can prevent all gas from cooling down (e.g., Mo & Mao 2002). The hot gas in the galactic halos can be either that heated up by supernovae explosions or that (re-)accreted during the accretion phase. The angular momentum of the hot gas may depend on the feedback mechanisms, but it is unknown how the feedback mechanism is operating in the universe. Nevertheless, our results clearly indicate that the angular momentum distribution of hot gas can be significantly

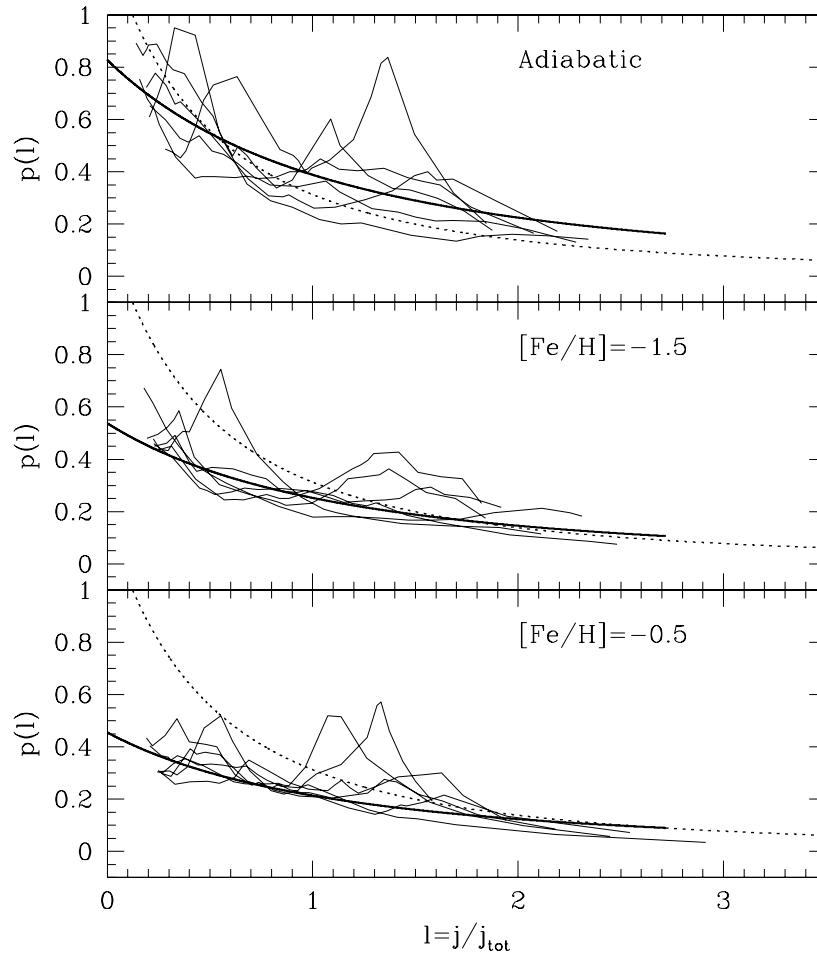


FIG. 11.—Angular momentum distributions of hot gas of six halos (*thin lines*) in each model. *Dotted thick lines*: Mean profile of B2001 for dark matter, $\mu = 1.25$. *Solid thick lines*: Mean profile of hot gas in our cooling models, $\mu = 1.8$, multiplied by the mean hot gas fraction 1, 0.65, and 0.55 from top to bottom panels for the right normalization. The figure can be compared to the observation of van den Bosch (2002) for disk galaxies. *Upper panel*: Nonradiative model. *Middle panel*: $[\text{Fe}/\text{H}] = -1.5$ model. *Lower panel*: $[\text{Fe}/\text{H}] = -0.5$ model.

different from that of dark matter and some simple heating mechanisms that prevent a fraction of gas from cooling down may successfully solve the angular momentum problem of disk galaxies.

Our above results appear to be inconsistent with a recent study of van den Bosch et al. (2002), who stress that the angular momentum distribution of hot gas is very similar to that of dark matter in their nonradiative simulation. As pointed out in § 2, they used the particle method to analyze the angular momentum distribution. In order to compare with their results, we have also carried out the same analysis as theirs. Examples of the angular momentum distributions $p(l)$ obtained in the particle method are shown in Figure 12, and the left column can be compared with Figure 6 of van den Bosch et al. (2002), where l is the scaled specific angular momentum $l = j/(R_{\text{vir}}V_{\text{vir}})$ as defined by van den Bosch et al. (2002) and $p(l)dl$ is the fraction of the particles that have the specific angular momentum in $l \sim l + dl$. From the figure, we see that $p(l)$ of gas component extends less to negative specific angular momentum than dark matter and embodies a sharper peak near zero. We also find a high fraction of mass, between 5% and 50%, that has negative specific momentum for all matter components, though this fraction is the lowest for hot gas component. Compared with the

results of van den Bosch et al. (2002), we find that our results are quantitatively in good agreement with theirs. This indicates that in spite of many differences between their simulation, and our simulations (simulation box, halo mass, analysis epoch, simulation codes, etc.), the angular momentum distributions are quite insensitive to the simulation details. The difference in the results between this study and their study must stem from the methods for computing the angular momentum profile. We adopt the cell method and they adopt the particle method. When the cell method is employed, the fraction of mass in counterrotation and the fraction of small j mass are significantly reduced at least for the hot gas. The reason might be that some local irregularities in the gas motion are smoothed out when the cell method is used. If these local irregularities, for example, correspond to the local shock motions, we believe that it is more appropriate to use the cell method to measure the angular momentum profile, because these irregularities will be later shocked away. But this point would certainly be worthy of a further investigation.

We would like to thank Gerhard Börner, Houjun Mo, Donghai Zhao, and especially Joel Primack for very helpful discussion and an anonymous referee for a detailed report

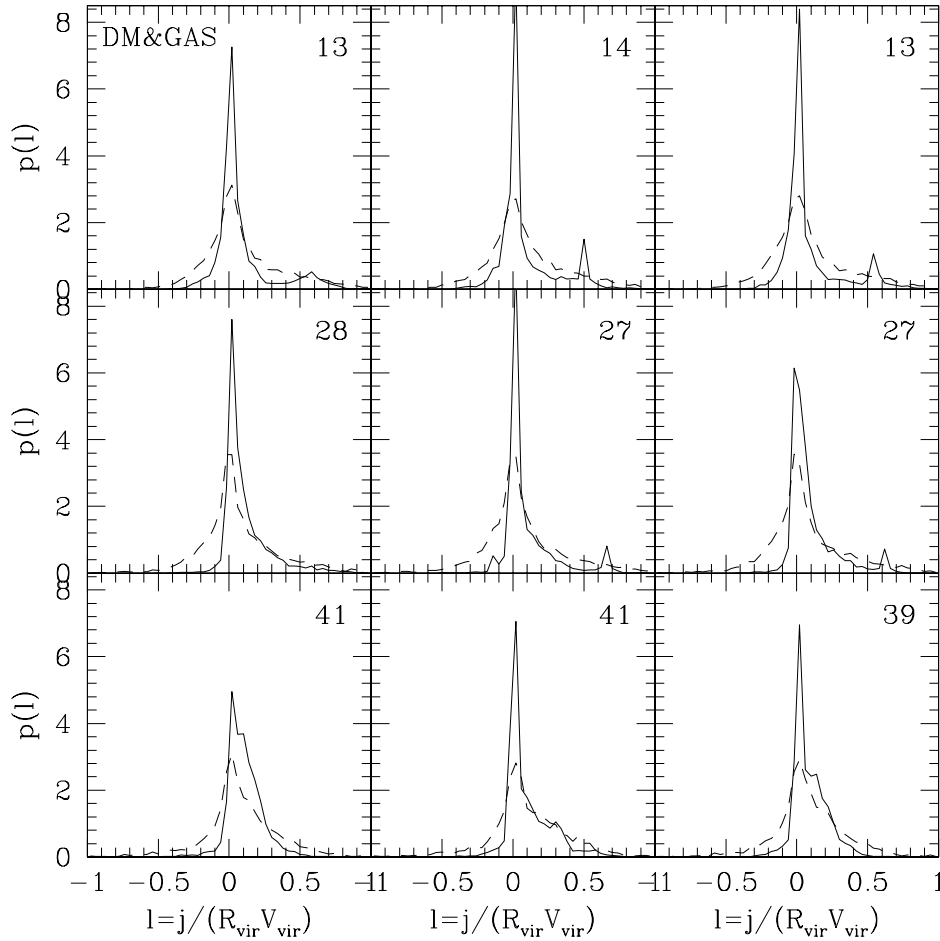


Fig. 12.—Angular momentum distributions of dark matter (*dashed lines*) and gas (*solid lines*) of three randomly selected halos in each model. *Left to right*: Nonradiative model, $[\text{Fe}/\text{H}] = -0.5$ model and $[\text{Fe}/\text{H}] = -1.5$ models, respectively. The halos in the same row of panels are the same halos, but they have experienced different cooling in the different cooling models.

that clarified many important points to us. The numerical simulations used in this paper were carried out at ADAC (the Astronomical Data Analysis Center) of the National

Astronomical Observatory, Japan. The work is supported in part by NKBRF (G19990754), and by NSFC (10043004).

REFERENCES

- Avila-Reese, V., & Firmani, C. 2000, *Rev. Mexicana Astron. Astrofis.*, 36, 23
- Barnes, J., & Efstathiou, G. 1987, *ApJ*, 319, 575
- Blumenthal, G. R., Faber, S. M., Flores, R., & Primack, J. R. 1986, *ApJ*, 301, 27
- Bryan, G. L., & Norman, M. L. 1998, *ApJ*, 495, 80
- Bullock, J. S., Dekel, A., Kolatt, T. S., Kravtsov, A. V., Klypin, A. A., Porciani, C., & Primack, J. R. 2001, *ApJ*, 555, 240 (B2001)
- Bullock, J. S., Kravtsov, A. V., & Colin, P. 2002, *ApJ*, 564, L1
- Catelan, P., & Theuns, T. 1996, *MNRAS*, 282, 455
- Chen, D. N., & Jing, Y. P. 2002, *MNRAS*, 336, 55
- Cole, S., Lacey, C. G., Baugh, C. M., & Frenk, C. S. 2000, *MNRAS*, 319, 168
- Cooray, A., & Chen, X. L. 2002, *ApJ*, 573, 43
- Dalcanton, J. J., Spergel, D. N., & Summers, F. J. 1997, *ApJ*, 482, 659
- de Jong, R. S., & Lacey, C. 2000, *ApJ*, 545, 781
- Doroshkevich, A. G. 1970, *Astrofizika*, 6, 581
- Fall, S. M., & Efstathiou, G. 1980, *MNRAS*, 193, 189
- Jimenez, R., Heavens, A. F., Hawkins, M. R. S., & Padoan, P. 1997, *MNRAS*, 292, L5
- Jing, Y. P., & Suto, Y. 2002, *ApJ*, 574, 538
- Kitayama, T., & Suto, Y. 1996, *ApJ*, 469, 480
- Knebe, A., Devriendt, J., Mahmood, A., & Silk, J. 2002, *MNRAS*, 329, 813
- Lee, J. H., & Pen, U.-L. 2000, *ApJ*, 532, 5
- . 2001, *ApJ*, 555, 106
- Lemson, G., & Kauffmann, G. 1999, *MNRAS*, 302, 111
- Mo, H. J., & Mao, S. 2002, *MNRAS*, 333, 768
- Mo, H. J., Mao, S., & White, S. D. M. 1998, *MNRAS*, 295, 319 (MMW)
- Peebles, P. J. E. 1969, *ApJ*, 155, 393
- Porciani, C., Dekel, A., & Hoffman, Y. 2002, *MNRAS*, 332, 339
- Shen, S. Y., Mo, H. J., White, S. D. M., Blanton, M. R., Kauffmann, G., Voges, W., Brinkmann, J., & Csabai, L. 2003, *MNRAS*, 343, 978
- Sutherland, R. S., & Dopita, M. A. 1993, *ApJS*, 88, 253
- van den Bosch, F. C. 1998, *ApJ*, 507, 601
- . 2001, *MNRAS*, 327, 1334
- . 2002, in *Rev Mexicana Astron. Astrofis. Conf. Ser., Galaxy Evolution, Theory, and Observations*, ed. V. Avila-Reese, C. Firmani, & C. Allen, (Mexico, DF: Inst. Astron. UNAM), 217, 139
- van den Bosch, F. C., Abel, T., Croft, R. A. C., Hernquist, L., & White, S. D. M. 2002, *ApJ*, 576, 21
- van den Bosch, F. C., Burkert, A., & Swaters, R. A. 2001, *MNRAS*, 326, 1205
- Wechsler, R. H., Bullock, J. S., Primack, J. R., Kravtsov, A. V., & Dekel, A. 2002, *ApJ*, 568, 52
- White, S. D. M., & Rees, M. J. 1978, *MNRAS*, 183, 341
- . 1984, *ApJ*, 286, 38
- Yoshikawa, K., Jing, Y. P., & Suto, Y. 2000, *ApJ*, 535, 593
- Yoshikawa, K., Taruya, A., Jing, Y. P., & Suto, Y. 2001, *ApJ*, 558, 520
- Zhao, D. H., Mo, H. J., Jing, Y. P., & Boerner, G. 2003, *MNRAS*, 338, 12